



1 **On the barium - oxygen consumption relationship in the Mediterranean Sea: implications**
2 **for mesopelagic marine snow remineralisation.**

3

4 Stéphanie H.M. Jacquet^{1*}, Dominique Lefèvre¹, Christian Tamburini¹, Marc Garel¹, Frédéric
5 A.C. Le Moigne¹, Nagib Bhairy¹, Marie Roumagnac¹, Sophie Guasco¹

6

7 ¹Aix Marseille Université, CNRS/INSU, Université de Toulon, IRD, Mediterranean Institute of
8 Oceanography (MIO), UM 110, 13288 Marseille, France

9

10 *Correspondence to: S. Jacquet (stephanie.jacquet@mio.osupytheas.fr)

11

12

13

14

15

16

17



18 **ABSTRACT**

19 In the ocean, remineralisation rate associated with sinking particles is a crucial variable. Since
20 the 90's, particulate biogenic barium (Ba_{xs}) has been used as an indicator of carbon
21 remineralization by applying a transfer function relating Ba_{xs} to O_2 consumption (Dehairs's
22 transfer function, Southern Ocean-based). Here, we tested its validity in the Mediterranean Sea
23 (ANTARES / EMSO-LO) for the first time by investigating connections between Ba_{xs} ,
24 prokaryotic heterotrophic production (PHP) and oxygen consumption (JO_2 -Opt; optodes
25 measurement). We show that: (1) higher Ba_{xs} (409 pM; 100- 500 m) in situations where
26 integrated PHP ($PHP_{100/500} = 0.90$) is located deeper, (2) higher Ba_{xs} with increasing JO_2 -Opt,
27 and (3) similar magnitude between JO_2 -Opt ($3.14 \text{ mmol m}^{-2} \text{ d}^{-1}$; 175- 450 m) and JO_2 -Ba (4.59
28 $\text{mmol m}^{-2} \text{ d}^{-1}$; transfer function). Overall, Ba_{xs} , PHP and JO_2 relationships follow trends observed
29 in the Southern Ocean. We believe that such transfer function could apply in the Mediterranean
30 Sea with no restriction.

31

32

33 **KEY WORDS:** particulate biogenic barium, mesopelagic zone, oxygen consumption,
34 prokaryotic heterotrophic production, carbon remineralization, Mediterranean Sea

35



36 1. INTRODUCTION

37 Ocean ecosystems play a critical role in the Earth's carbon (C) cycle [IPCC, 2014]. The
38 quantification of their impacts of both present conditions and future predictions remains one of
39 the greatest challenges in oceanography [Siegel et al., 2016]. In essence, the biological C pump is
40 termed for the numerous processes involved in maintaining the vertical gradient in dissolved
41 inorganic C. This includes processes such as organic matter production in surface, its export and
42 subsequent remineralization. Most of marine snow organic C conversion (i.e. remineralization)
43 into CO₂ by heterotrophic organisms (i.e. respiration) occurs in the mesopelagic zone (100-1000
44 m) [Martin et al., 1987; Buesseler and Boyd, 2009]. Globally, the flux of C exported below 1000
45 m depth is the key determinant of ocean carbon storage capacity [Henson et al., 2011]. However,
46 there is no consensus on C transfer efficiency estimations from field experiments, leading to an
47 imbalance of the water column C budget [Giering et al., 2014]. Resolving this imbalance is in the
48 core of numerous studies in the global ocean, but also regionally, especially in the Mediterranean
49 Sea (MedSea). Due to limited exchanges with adjacent basin and the existence of an intense
50 overturning circulation qualitatively resembling the global one (but with shorter time scales), the
51 MedSea is often considered as a laboratory to observe and understand the impact of transient
52 climate variability on ecosystems and biogeochemical cycles [Malanotte-Rissoli et al., 2014]. In a
53 context of climate changes, better constraining C fluxes and the ocean C storage capacity is of
54 crucial importance.

55 Particulate barium in excess (Ba_{xs}, i.e. biogenic Ba from total particulate Ba after correction for
56 lithogenic Ba) is a geochemical tracer of particulate organic carbon (POC) remineralization in the
57 mesopelagic layer [Dehairs et al., 1997]. Ba_{xs} mostly occurs in the form of barite microcrystals
58 (BaSO₄) at these depths. In a global ocean undersaturated with respect to barite, studies report
59 that Ba_{xs} would precipitate inside oversaturated biogenic micro-environments during POC



60 degradation by heterotrophic prokaryotes in the mesopelagic zone, through sulfate and/or barium
61 enrichment [Bertram and Cowen, 1997]. The first-ever studies on mesopelagic Ba_{xs} reported
62 coinciding Ba_{xs} maxima with depths of dissolved O_2 minimum and pCO_2 maximum [Dehairs et
63 al., 1987, 1997]. By using an 1D advection-diffusion model applied to highly resolved, precise
64 O_2 profiles in the Atlantic sector of the Southern Ocean (ANTX/6 cruise; Shopova et al., 1995),
65 Dehairs et al. [1997] established an algorithm converting mesopelagic Ba_{xs} concentration into O_2
66 consumption rate (JO_2) and organic C remineralized (POC remineralization rate). This transfer
67 function has been widely used until now [Cardinal et al., 2001- Lemaitre et al., 2018]. Yet its
68 validity has never been tested in other oceanic provinces. Recently, significant progresses were
69 made in relating Ba_{xs} , O_2 dynamics to prokaryotic heterotrophic activity [Jacquet et al., 2015].
70 Nevertheless, the Dehairs transfer function has never been revised since. These advancements
71 clearly show that Ba_{xs} is closely related with the vertical distribution of prokaryotes heterotrophic
72 production (PHP) (the rate of change with depth), reflecting the temporal progression of POC
73 remineralization processes. Also, in a first attempt to test the validity of the Dehairs's transfer
74 function in other locations, Jacquet et al. [2015] confronted oxygen consumption rates (JO_2) from
75 direct measurements (dark community respiration, DCR) to derived JO_2 from Ba_{xs} data (using the
76 transfer function) in the Kerguelen area (Indian sector of the Southern Ocean). We revealed good
77 convergence of JO_2 rates from these two approaches, further supporting the Dehairs's function to
78 estimate POC remineralization rates in different biogeochemical settings of the Southern Ocean.

79 Here, we further investigate relationships between the mesopelagic Ba_{xs} proxy, prokaryotic
80 activity and oxygen dynamics (Figure 1a) in the northwestern Mediterranean Sea (MedSea), a
81 different biogeochemical setting to those already studied (see references above). Today,
82 observations of the various components of the MedSea biological C pump provide organic C
83 fluxes varying by at least an order of magnitude [Santinelli et al., 2010; Ramondenc et al., 2016].



84 Malanotte-Rissoli et al. [2014] reviewing unsolved issues and future directions for MedSea
85 research highlighted the need to further investigate biogeochemical processes at intermediate
86 (mesopelagic) and deep layers to reconcile the C budget in the Mediterranean basin. Previous
87 particulate Ba_{xs} dataset is very scarce in the NW- MedSea, with in general very low vertical
88 sampling resolution [Sanchez Vidal et al., 2005] or very restricted studied areas [Dehairs et al.,
89 1987; Sternberg et al., 2008]. Here we discuss Ba_{xs} , PHP and JO_2 (from optodes measurement
90 during incubations) at the ANTARES / EMSO-LO observatory site (Figure 1a, b). We
91 hypothesize that the Dehairs's transfer function converting Ba_{xs} into POC remineralization also
92 applies in a different ocean ecosystem functioning from the Southern Ocean. We suggest that the
93 Ba_{xs} proxy can be used as routine tracer to estimate local-scale processes of mesopelagic POC
94 remineralization in the Mediterranean basin.

95

96 **2. SAMPLING AND ANALYSES**

97 **2.1 STUDY SITE**

98 The BATMAN cruise (<https://doi.org/10.17600/16011100>, March 10-16 2016, *R/V EUROPE*)
99 took place to the ANTARES / EMSO-LO observatory site (42°48'N, 6°10'E; Tamburini et al.,
100 2013), 40 km off the coast of Toulon, southern France (Figure 1b). The hydrological and
101 biogeochemical conditions at this site are monitored monthly in the framework of the MOOSE
102 (Mediterranean Ocean Observing System for the Environment) program and of the EMSO
103 (European Multidisciplinary Subsea Observatory) observation program. The hydrography
104 displays the general three-layer MedSea system with surface, intermediate and deep waters
105 [Hainbucher et al., 2014]. Briefly, the main water masses can be distinguished (see potential
106 temperature – salinity diagram during the BATMAN cruise in Figure 1c): (1) Surface Water
107 (SW); (2) Winter Intermediate Water (WIW) and Levantine Intermediate water (LIW). LIW is



108 present at intermediate depths (around 400 m at ANTARES) and is characterized by temperature
109 and a salinity maxima; (4) Mediterranean Deep Water (MDW).

110

111 2.2 ANALYSES

112 For particulate barium, 4 to 7 L of seawater sampled using Niskin bottles were filtered onto 47
113 mm polycarbonate membranes (0.4 μm porosity) under slight overpressure supplied by filtered
114 air. Filters were rinsed with few mL of Milli-Q grade water to remove sea salt, dried (50°C) and
115 stored in Petri dishes. Thirteen depths between surface and 2000 m were sampled by combining
116 different casts sampled closeby in time and space (total of 28 samples). In the laboratory, we
117 performed a total digestion of filters using a tri-acid (0.5 mL HF /1.5 mL HNO₃ / HCl 1 mL; all
118 Optima grade) mixture in closed teflon beakers overnight at 95°C in a clean pressurized room.
119 After evaporation close to dryness, samples were re-dissolved into 10 mL of HNO₃ 2%. The
120 solutions were analysed for Ba and other elements of interest (Na and Al) by HR-ICP-MS (High
121 Resolution-Inductively Coupled Plasma- Mass Spectrometry; ELEMENT XR ThermoFisher).
122 Details on sample processing and analysis are given in Cardinal et al. [2001] and Jacquet et al.
123 [2015]. The presence of sea-salt was checked by analysing Na and the sea-salt particulate Ba
124 contribution was found negligible. Particulate biogenic barium in excess (hereafter referred to as
125 Ba_{xs}) was calculated as the difference between total Ba and lithogenic Ba using Al as the
126 lithogenic reference element [Taylor and Mc.Lennan, 1985]. The standard uncertainty [Ellison et
127 al., 2000] on Ba_{xs} concentration ranges between 5.0 and 5.5%. The term “in excess” is used to
128 indicate that concentrations are larger than the Ba_{xs} background. The background (or residual
129 value) is considered as “preformed” Ba_{xs} at zero oxygen consumption left over after transfer and
130 partial dissolution of Ba_{xs} produced during degradation of previous phytoplankton growth events.



131 Oxygen concentrations were measured using optical oxygen sensor (Aanderaa 4330-Optodes)
132 at 4 depths in the mesopelagic layer (175, 250, 450 and 1000 m). In total each of the 8 optodes
133 (two per depths) were placed into a sealed 1L borosilicate glass bottles incubated at a fixed
134 temperature of 13°C in thermo-regulated baths for 24 to 48 hours. Oxygen consumption rates
135 (later referred to as JO_2 -Opt) were calculated from oxygen concentration evolution with time
136 applying linear model calculations.

137 Prokaryotic heterotrophic production (PHP) estimation was measured over time course
138 experiments at *in situ* temperature (13°C) following the protocol described in Tamburini et al.
139 [2002]. 3H -leucine labelled tracer [Kirchman, 1993] was used. To calculate prokaryotic
140 heterotrophic production, we used the empirical conversion factor of 1.55 ng C per pmol of
141 incorporated leucine according to Simon and Azam [1989], assuming that isotope dilution was
142 negligible under these saturating concentrations.

143

144 **3. RESULTS AND DISCUSSION**

145 **3.1 Barium vertical distribution**

146 Particulate biogenic Ba_{xs} , particulate Al (pAl) and biogenic Ba fraction profiles in the upper
147 1000 m at ANTARES are reported in Figure 2a. Ba_{xs} concentrations range from 12 to 719 pM.
148 The biogenic Ba fraction range from 51 to 91 % of the total particulate Ba signal. Particulate Al
149 concentrations (pAl) are low and range from 8 to 170 nM. Ba_{xs} concentrations are low in surface
150 water (<100 pM) where the lithogenic fraction reaches 43 to 49 % in the upper 70 m. From
151 previous studies we know that Ba_{xs} in surface waters is distributed over different, mainly non-
152 barite biogenic phases, and incorporated into or adsorbed onto phytoplankton material. As such
153 these do not reflect POC remineralization processes, in contrast to mesopelagic waters where
154 Ba_{xs} is mainly composed of barite formed during prokaryotic degradation of organic matter. At



155 ANTARES the Ba_{xs} profile displays a mesopelagic Ba_{xs} maximum between 100 and 500 m,
156 reaching up to 719 pM at 175 m. Ba is mostly biogenic at these depths ($> 80\%$). Ba_{xs}
157 concentrations then decrease below 500 m to reach a background value of around 130 pM (see
158 BKG in Figure 2). Note that the MedSea is largely undersaturated with respect to barite, with
159 saturation state ranging between 0.2 and 0.6 over the basin [Jacquet et al., 2016; Jullion et al.,
160 2017]. For comparison, the Ba background value in the Southern Ocean reaches 180 to 200 pM
161 below 1000 m [Dehairs et al., 1997; Jacquet et al. 2015]. Previously, Sternberg et al. [2008]
162 reported the seasonal evolution of Ba_{xs} profiles at the DYFAMED station ($43^{\circ}25'N-7^{\circ}52'E$;
163 BARMED project) northeast from ANTARES (Figure 1c) in the NW-MedSea. The present Ba_{xs}
164 profile at ANTARES (March 2016) is very similar to the Ba_{xs} profile measured in March 2003 at
165 DYFAMED (Figure 2a). The slight difference between Ba_{xs} profiles in the upper 75 m suggests
166 more Ba bounded and/or adsorbed onto phytoplankton material during BARMED. Both profiles
167 present a Ba_{xs} maximum in the upper mesopelagic zone between 150 and 200 m. Below this
168 maximum, Ba_{xs} concentrations gradually decrease to reach around 130 pM between 500 and
169 1000 m (this study). A similar value was reached between 500 and 600 m at the DYFAMED
170 station over the whole studied period (between February and June 2003; Sternberg et al., 2008).

171

172 **3.2 Prokaryotic heterotrophic production**

173 The particulate excess Ba ($>BKG$) is centred in the upper mesopelagic zone between 100 and
174 500 m and reflects that POC remineralization mainly occurred at these depths (Figure 2a). Depth-
175 weighted average (DWA) Ba_{xs} content (409 pM) was calculated over this entire depth interval.
176 Figure 2b shows column-integrated PHP at 100 m over column-integrated PHP at 500 m
177 ($PHP_{100/500} = 0.90$), according to the relationship obtained during KEOPS1 (summer) and
178 KEOPS2 (spring; out plateau stations) cruises in the Southern Ocean [Jacquet et al., 2008; 2015]



179 and #DY032 cruise (2015, *R/V DISCOVERY*) at the PAP (Porcupine Abyssal Plain) observatory
180 in the northeast Atlantic (49°N, 16.5 °W) (personal data). Results at the ANTARES / EMSO-LO
181 site follow the trend previously reported in the Southern Ocean, indicating higher DWA Ba_{xs} in
182 situations where a significant part of column-integrated PHP is located deeper in the water
183 column (high Int. $PHP_{x1}/IntPHP_{x2}$ ratio; Figure 2b). These previous studies revealed that the
184 shape of the column-integrated PHP profile (i.e. the attenuation gradient) is important in setting
185 the Ba_{xs} signal in the mesopelagic zone (Dehairs et al., 2008; Jacquet et al., 2008, 2015]. Indeed,
186 mesopelagic Ba_{xs} appears reduced when most of the column-integrated PHP is limited to the
187 upper layer (indicating an efficient remineralization in surface), compared to situations where a
188 significant part of integrated PHP is located deeper in the water column (reflecting significant
189 deep PHP activity, POC export and subsequent remineralization) (Figure 2b). Our MedSea
190 results are located along the trend defined in the Southern Ocean during KEOPS1 cruise. It is
191 generally considered that Ba_{xs} (barite) forms inside sulfate and/or barium oversaturated biogenic
192 micro-environments during POC degradation by heterotrophic prokaryotes. However, it is
193 unclear whether barite formation at mesopelagic depths is (directly or indirectly) bacterially
194 induced or bacterially influenced. Overall, our results strengthen the close link between the water
195 column Ba_{xs} distribution and respiration (organic matter degradation).

196

197 **3.3 Oxygen- barium relationship**

198 The relationship we obtained at ANTARES between Ba_{xs} concentrations and oxygen
199 consumption rates from optodes measurements (JO_2 -Opt) is reported in Figure 3a. JO_2 -Opt range
200 from 0.11 to 5.85 $\mu\text{mol L}^{-1} \text{d}^{-1}$. The relationship indicates higher Ba_{xs} concentrations with
201 increasing JO_2 -Opt. An interesting feature is the intercept at zero JO_2 -Opt (around 128 pM)



202 which further supports the Ba BKG value at ANTARES (130 pM) determined from measured
203 Ba_{xs} profiles (Figure 3a).

204 We applied a similar approach as reported in Jacquet et al. (2015) where we show the
205 correlation between JO₂ obtained from dark community respiration DCR (winkler titration; JO₂-
206 DCR) data integration in the water column and JO₂ based on Ba_{xs} content (Dehairs's transfer
207 function; later referred to as JO₂-Ba). Similarly, to estimate JO₂-Ba in the present study we used
208 the following equation [Dehairs et al., 1997]:

$$209 \quad \text{JO}_2\text{-Ba} = (\text{Ba}_{\text{xs}} - \text{Ba BKG}) / 17450 \quad (1)$$

210 A Ba BKG value of 130 pM was used (see above). JO₂-Ba is confronted to JO₂-Opt integrated
211 over the same layer depth (between 175 and 450 m; Figure 3b). JO₂ rates are of the same order of
212 magnitude (JO₂-Ba = 4.59 mmol m⁻² d⁻¹ and JO₂-opt = 3.14 mmol m⁻² d⁻¹). The slight difference
213 could be explained by the integration time of both methods: few hours to days for the incubations
214 vs. few days to weeks for Ba_{xs} (seasonal build-up; Jacquet et al., 2007). JO₂ rates calculated in the
215 present work are 3 times higher than those reported in the Southern Ocean during KEOPS1
216 [Jacquet et al., 2015] but they are in good agreement with the Ba_{xs} vs JO₂ trend (Figure 3b).
217 Overall, our results indicate similar Ba_{xs} - JO₂ relationship in the Southern Ocean and the
218 Mediterranean Sea. This further supports the universal validity of the Dehairs's transfer function
219 in the present study.

220

221 **3.4 Estimated particles remineralisation rates and implications**

222 In order to provide a Ba_{xs}-derived estimate of POC remineralization rate (MR) at the
223 ANTARES / EMSO-LO observatory during BATMAN cruise, we converted JO₂-Ba into C
224 respired using the Redfield (RR) C/O₂ molar ratio (127/175; Broecker et al., 1985) multiplied by
225 the depth layer considered (Z) [Dehairs et al., 1997]:



226 $MR = Z \times JO_2 - Ba \times RR \quad (2)$

227 We obtain a POC remineralization rate of $11 \text{ mmol C m}^{-2} \text{ d}^{-1}$ (10% RSD). This is within the
228 range of previously published remineralization fluxes in the Mediterranean Sea from sediment
229 trap [Sanchez-Vidal et al., 2005] and from thorium-derived data [Speicher et al., 2006]. It is also
230 in good agreement with recent POC flux attenuation combining drifting sediment traps and
231 underwater vision profilers [Ramondenc et al., 2016].

232 The present paper brings a first insight into the connections of Ba_{xs} , PHP and JO_2 at the
233 ANTARES/EMSO-LO observatory site in the northwestern Mediterranean Sea during the
234 BATMAN (2016) cruise. Our results reveal a strong relationship between Ba_{xs} contents and
235 measured JO_2 rates. Also, DWA Ba_{xs} vs. column integrated PHP, as well as measured vs. Ba_{xs} -
236 based JO_2 relationships follow trends previously reported in the Southern Ocean where the
237 Dehairs's function was first established to estimate POC remineralisation rate. Results from the
238 present study would indicate that this function can also be applied in the Mediterranean basin
239 provided that adequate Ba_{xs} background values are estimated. From a global climate perspective,
240 the Ba_{xs} tool will help to better balance the MedSea water column C budget. It will contribute to
241 gain focus on the emerging picture of the C transfer efficiency (strength of the biological pump).

242

243 **ACKNOWLEDGEMENTS**

244 We thank the officers and crew of *R/V EUROPE* for their assistance during work at sea. This
245 research was supported by the French national LEFE/INSU "REPAP" project (PI. S. Jacquet). It
246 was co-funded by the "ROBIN" project (PIs. C. Tamburini, F.A.C. Le Moigne) of Labex OT-
247 Med (ANR-11-LABEX-0061) funded by the Investissements d'Avenir and the French
248 Government project of the ANR, through the A*Midex project (ANR-11-IDEX-0001-02).
249 Authors have benefited of the support of the SNO-MOOSE and SAM-MIO. BATMAN is a



250 contribution to the "AT – POMPE BIOLOGIQUE" of the Mediterranean Institute of
251 Oceanography (MIO) and to the international IMBER program. The instrument (ELEMENT XR,
252 ThermoFisher) was supported in 2012 by European Regional Development Fund (ERDF).

253



254 **Figure captions**

255 Figure 1: (a) Schematic representation of the convergence of the different estimators of oxygen
256 consumption and C remineralization rates from the “oxygen dynamics”, “barium proxy” and
257 “prokaryotic activity” tools; (b) Location of the BATMAN cruise at the ANTARES observatory
258 site in the NW-Mediterranean Sea (42°48’N, 6°10’E); (b) Potential temperature - salinity - depth
259 plots and isopycnals for BATMAN profiles. SW : Surface Water, WIW : Winter Intermediate
260 Water, LIW : Levantine Intermediate Water, DMW : Deep Mediterranean Water. Graph
261 constructed using Ocean Data View (Schlitzer, 2002; Ocean Data View; [http://www.awi-
262 bremerhaven.de/GEO/ODV](http://www.awi-
262 bremerhaven.de/GEO/ODV))

263

264 Figure 2: (a) Particulate biogenic Ba_{xs} (pM) and particulate Al (nM) profiles next to the biogenic
265 Ba fraction (%) in the upper 1000 m at ANTARES. The grey area represents a biogenic Ba
266 fraction larger than 80 %. BKG: Ba_{xs} background. Ba_{xs} profile (pM) at DYFAMED : data from
267 Sternberg et al. (2008); (b) ANTARES ratio plot (green square) of integrated PHP in the upper
268 100 m over integrated PHP in the upper 500 m versus depth-weighted average (DWA)
269 mesopelagic Ba_{xs} (pM) over the 150- 500 depth interval. Regression of the same ratio is reported
270 for KEOPS1 (out plateau stations) and KEOPS2 (Southern Ocean; Jacquet et al., 2015) and
271 #DY032 (PAP station, NE-Atlantic; pers. data) cruises.

272

273 Figure 3: (a) Relationship between Ba_{xs} concentrations (pM) and oxygen consumption rates
274 ($\mu\text{mol L}^{-1} \text{d}^{-1}$) from optodes measurements ($\text{JO}_2\text{-Opt}$) at ANTARES; (b) Confrontation of oxygen
275 consumption rates ($\text{mmol m}^{-2} \text{d}^{-1}$) obtained from different methods: optodes measurements (this
276 work), dark community respiration DCR (winkler titration; $\text{JO}_2\text{-DCR}$; Jacquet et al., 2015;



277 KEOPS1), and (Dehairs's transfer function calculation based on Ba_{xs} content (Dehairs et al.,
278 1997).
279



280 **References**

- 281 Bertram, Miriam, and James P. Cowen. “Morphological and Compositional Evidence for Biotic
282 Precipitation of Marine Barite.” *Journal of Marine Research* 55 (1997): 577–93.
- 283 Broecker, Wallace S. “‘NO’, a Conservative Water-Mass Tracer.” *Earth and Planetary Science
284 Letters* 23, no. 1 (August 1974): 100–107. doi:10.1016/0012-821X(74)90036-3.
- 285 Buesseler, Ken O., and Philip W. Boyd. “Shedding Light on Processes That Control Particle
286 Export and Flux Attenuation in the Twilight Zone of the Open Ocean.” *Limnology and
287 Oceanography* 54, no. 4 (2009): 1210–32. doi:10.4319/lo.2009.54.4.1210.
- 288 Cardinal, Damien, Frank Dehairs, Thierry Cattaldo, and Luc André. “Geochemistry of Suspended
289 Particles in the Subantarctic and Polar Frontal Zones South of Australia: Constraints on
290 Export and Advection Processes.” *Journal of Geophysical Research: Oceans* 106, no. C12
291 (décembre 2001): 31637–56. doi:10.1029/2000JC000251.
- 292 Dehairs, F., R. Chesselet, and J. Jedwab. “Discrete Suspended Particles of Barite and the Barium
293 Cycle in the Open Ocean.” *Earth and Planetary Science Letters* 49, no. 2 (September 1980):
294 528–50. doi:10.1016/0012-821X(80)90094-1.
- 295 Dehairs, F., S. Jacquet, N. Savoye, B. A. S. Van Mooy, K. O. Buesseler, J. K. B. Bishop, C. H.
296 Lamborg, et al. “Barium in Twilight Zone Suspended Matter as a Potential Proxy for
297 Particulate Organic Carbon Remineralization: Results for the North Pacific.” *Deep Sea
298 Research Part II: Topical Studies in Oceanography*, Understanding the Ocean’s Biological
299 Pump: results from VERTIGO, 55, no. 14–15 (juillet 2008): 1673–83.
300 doi:10.1016/j.dsr2.2008.04.020.



- 301 Dehairs, F., C. E. Lambert, R. Chesselet, and N. Risler. “The Biological Production of Marine
302 Suspended Barite and the Barium Cycle in the Western Mediterranean Sea.”
303 *Biogeochemistry* 4, no. 2 (June 1, 1987): 119–40. doi:10.1007/BF02180151.
- 304 Dehairs, F., D. Shopova, S. Ober, C. Veth, and L. Goeyens. “Particulate Barium Stocks and
305 Oxygen Consumption in the Southern Ocean Mesopelagic Water Column during Spring and
306 Early Summer: Relationship with Export Production.” *Deep Sea Research Part II: Topical
307 Studies in Oceanography* 44, no. 1–2 (1997): 497–516. doi:10.1016/S0967-0645(96)00072-
308 0.
- 309 Ellison, Eurachem/CITAC Guide CG4, Quantifying Uncertainty in Analytical Measurement.
310 Eds. S.L.R. Ellison, M. Rosslein and A. Williams. Second edition ISBN 0948926 15 5, Pp
311 120, 2000.
- 312 Giering, Sarah L. C., Richard Sanders, Richard S. Lampitt, Thomas R. Anderson, Christian Tamburini,
313 Mehdi Boutrif, Mikhail V. Zubkov, et al. “Reconciliation of the Carbon Budget in the Ocean’s
314 Twilight Zone.” *Nature* 507, no. 7493 (March 27, 2014): 480–83.
- 315 Hainbucher, D., A. Rubino, V. Cardin, T. Tanhua, K. Schroeder, and M. Bensi. “Hydrographic
316 Situation during Cruise M84/3 and P414 (spring 2011) in the Mediterranean Sea.” *Ocean
317 Sci.* 10, no. 4 (juillet 2014): 669–82. doi:10.5194/os-10-669-2014.
- 318 Henson, Stephanie A., Richard Sanders, Esben Madsen, Paul J. Morris, Frédéric Le Moigne, and
319 Graham D. Quartly. “A Reduced Estimate of the Strength of the Ocean’s Biological Carbon
320 Pump.” *Geophysical Research Letters* 38, no. 4 (février 2011): L04606.
321 doi:10.1029/2011GL046735.



- 322 IPCC Working Group 1, 5th Assessment Report (AR5) Climate Change 2013, Published in Jan. 2014.
- 323 Jacquet, S. H. M., F. Dehairs, D. Lefèvre, A. J. Cavagna, F. Planchon, U. Christaki, L. Monin, L.
324 André, I. Closset, and D. Cardinal. “Early Spring Mesopelagic Carbon Remineralization and
325 Transfer Efficiency in the Naturally Iron-Fertilized Kerguelen Area.” *Biogeosciences* 12, no.
326 6 (March 17, 2015): 1713–31. doi:10.5194/bg-12-1713-2015.
- 327 Jacquet, S. H. M., F. Dehairs, N. Savoye, I. Obernosterer, U. Christaki, C. Monnin, and D.
328 Cardinal. “Mesopelagic Organic Carbon Remineralization in the Kerguelen Plateau Region
329 Tracked by Biogenic Particulate Ba.” *Deep Sea Research Part II: Topical Studies in*
330 *Oceanography*, KEOPS: Kerguelen Ocean and Plateau compared Study, 55, no. 5–7 (March
331 2008): 868–79. doi:10.1016/j.dsr2.2007.12.038.
- 332 Jacquet, S. H. M., J. Henjes, F. Dehairs, A. Worobiec, N. Savoye, and D. Cardinal. “Particulate
333 Ba-Barite and Acantharians in the Southern Ocean during the European Iron Fertilization
334 Experiment (EIFEX).” *Journal of Geophysical Research* 112, no. G4 (October 23, 2007).
335 doi:10.1029/2006JG000394.
- 336 Jacquet, S.H.M., C. Monnin, V. Riou, L. Jullion, and T. Tanhua. “A High Resolution and Quasi-
337 Zonal Transect of Dissolved Ba in the Mediterranean Sea.” *Marine Chemistry* 178 (January
338 20, 2016): 1–7. doi:10.1016/j.marchem.2015.12.001.
- 339 Jullion, L., S. H. M. Jacquet, and T. Tanhua. “Untangling Biogeochemical Processes from the
340 Impact of Ocean Circulation: First Insight on the Mediterranean Dissolved Barium
341 Dynamics.” *Global Biogeochemical Cycles* 31, no. 8 (2017): 1256–70.
342 doi:10.1002/2016GB005489.



- 343 Kirchman DL (1993) Leucine incorporation as a measure of biomass production by heterotrophic
344 bacteria. In: Kemp PF, Sherr BF, Sherr EB, Cole JJ (eds) Handbooks of methods in aquatic
345 microbial ecology. Lewis Publishers, Boca Raton, Ann Arbor, London, Tokyo, p 509–512
- 346 Lemaitre, N., H. Planquette, F. Planchon, G. Sarthou, S. Jacquet, M. I. García-Ibáñez, A.
347 Gourain, et al. “Particulate Barium Tracing of Significant Mesopelagic Carbon
348 Remineralisation in the North Atlantic.” *Biogeosciences* 15, no. 8 (2018): 2289–2307.
349 doi:10.5194/bg-15-2289-2018.
- 350 Malanotte-Rizzoli, P., V. Artale, G. L. Borzelli-Eusebi, S. Brenner, A. Crise, M. Gacic, N. Kress,
351 et al. “Physical Forcing and Physical/biochemical Variability of the Mediterranean Sea: A
352 Review of Unresolved Issues and Directions for Future Research.” *Ocean Science* 10, no. 3
353 (2014): 281–322. doi:10.5194/os-10-281-2014.
- 354 Martin, John H., George A. Knauer, David M. Karl, and William W. Broenkow. “VERTEX:
355 Carbon Cycling in the Northeast Pacific.” *Deep Sea Research Part A. Oceanographic
356 Research Papers* 34, no. 2 (1987): 267–85. doi:http://dx.doi.org/10.1016/0198-
357 0149(87)90086-0.
- 358 Ramondenc, Simon, Goutx Madeleine, Fabien Lombard, Chiara Santinelli, Lars Stemmann,
359 Gabriel Gorsky, and Lionel Guidi. “An Initial Carbon Export Assessment in the
360 Mediterranean Sea Based on Drifting Sediment Traps and the Underwater Vision Profiler
361 Data Sets.” *Deep Sea Research Part I: Oceanographic Research Papers* 117 (November
362 2016): 107–19. doi:10.1016/j.dsr.2016.08.015.



- 363 Sanchez-Vidal, A., R. W. Collier, A. Calafat, J. Fabres, and M. Canals (2005), Particulate barium
364 fluxes on the continental margin: A study from the Alboran Sea (Western Mediterranean),
365 *Mar. Chem.*, 93, 105–117.
- 366 Santinelli, Chiara, Luciano Nannicini, and Alfredo Seritti. “DOC Dynamics in the Meso and Bathypelagic
367 Layers of the Mediterranean Sea.” *Deep Sea Research Part II: Topical Studies in Oceanography*,
368 *Ecological and Biogeochemical Interactions in the Dark Ocean*, 57, no. 16 (août 2010): 1446–59.
369 doi:10.1016/j.dsr2.2010.02.014.
- 370 Siegel DA, Buesseler KO, Behrenfeld MJ, Benitez-Nelson CR, Boss E, Brzezinski MA, Burd A, Carlson
371 CA, D'Asaro EA, Doney SC, Perry MJ, Stanley RHR and Steinberg DK (2016) Prediction of the
372 Export and Fate of Global Ocean Net Primary Production: The EXPORTS Science Plan. *Front. Mar.*
373 *Sci.* 3:22. doi: 10.3389/fmars.2016.00022
- 374 Simon M, Azam F (1989) Protein content and protein synthesis rates of planktonic marine
375 bacteria. *Mar Ecol Prog Ser* 51:201–213
- 376 Shopova, D., F. Dehairs, and W. Baeyens. “A Simple Model of Biogeochemical Element
377 Distribution in the Oceanic Water Column.” *Journal of Marine Systems* 6, no. 4 (juin 1995):
378 331–44. doi:10.1016/0924-7963(94)00032-7.
- 379 Speicher, E. A., S. B. Moran, A. B. Burd, R. Delfanti, H. Kaberi, R. P. Kelly, C. Papucci, et al.
380 “Particulate Organic Carbon Export Fluxes and Size-Fractionated POC/234Th Ratios in the
381 Ligurian, Tyrrhenian and Aegean Seas.” *Deep Sea Research Part I: Oceanographic*
382 *Research Papers* 53, no. 11 (2006): 1810–30.
383 doi:http://dx.doi.org/10.1016/j.dsr.2006.08.005.



384 Sternberg, E., C. Jeandel, E. Robin, and M. Souhaut. “Seasonal Cycle of Suspended Barite in the
385 Mediterranean Sea.” *Geochimica et Cosmochimica Acta* 72, no. 16 (2008): 4020–34.
386 doi:<https://doi.org/10.1016/j.gca.2008.05.043>.

387 Tamburini C, Canals M, Durieu de Madron X, Houpert L, Lefèvre D, Martini S, D’Ortenzio F,
388 Robert A, Testor P, and the ANTARES collaboration (2013) Deep-sea bioluminescence
389 blooms after dense water formation at the ocean surface. PLoS One 8:e67523

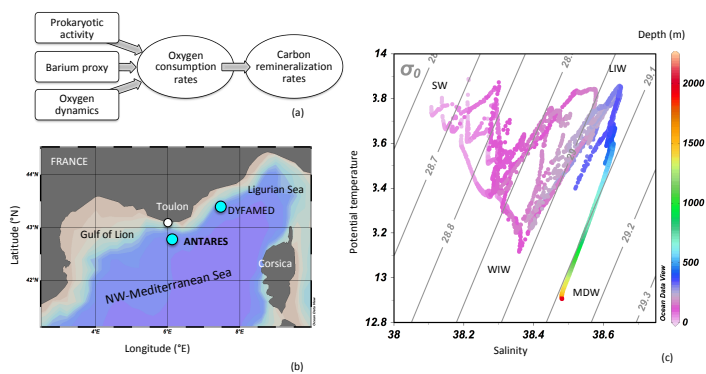
390 Tamburini C, Garcin J, Ragot M, Bianchi A (2002) Biopolymer hydrolysis and bacterial
391 production under ambient hydrostatic pressure through a 2000 m water column in the NW
392 Mediterranean. Deep Res II 49:2109–2123

393 Taylor, S.R., McLennan, S.M.: The continental crust: its composition and evolution, Blackwell
394 Scientific Publications, 312pp, 1985.

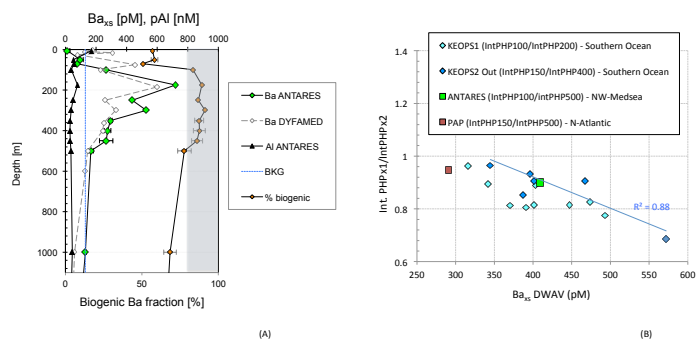
395



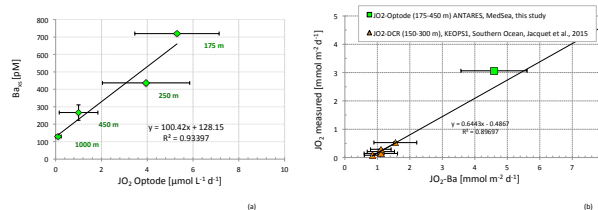
396 Figure 1



397
398



399 Figure 2



400 Figure 3
401